Global Conformal Parameterization via an Implementation of Holomorphic Quadratic Differentials

Hui Zhao, Shaodong Wang, and Wencheng Wang

Abstract—We propose an algorithm to compute global conformal parameterizations of high-genus meshes, which is based on an implementation of holomorphic quadratic differentials. First, we design a novel diffusion method which is capable of computing a *pole-free* discrete *harmonic* measured foliation. Second, we propose a definition for *discrete* holomorphic quadratic differential which consists of a horizontal and a vertical *harmonic* measured foliation. Third, we present a practical algorithm to approximate the *discrete natural coordinates* for a holomorphic quadratic differential, which represents a flat metric with cones conformal to the original metric, i.e., a parameterization. Finally, we apply the *discrete natural coordinates* for parameterization of high genus meshes. Our parameterization method is *global conformal* and simple to implement. The advantage of our method over the approach based on holomorphic differential one-forms is that ours has a larger space of parameterizations. We demonstrate our approach with hundreds of configurations on dozens of meshes to show its robustness on conformal parameterization.

Index Terms—foliation, parameterization, differential one-form, holomorphic quadratic differential, harmonic

1 Introduction

Mesh parameterization is a challenging problem in geometry processing. There are already many powerful algorithms for disk-type meshes [1]. However, for high-genus ones, creating a global conformal parameterizations is still hard to achieve. In this paper, we address this challenge based on holomorphic quadratic differentials.

A flat metric with cones leads to a global parameterization [2]. And if the flat metric is conformal, the map will be conformal as well. For example, it is proposed to use two independent harmonic one-forms on a mesh [3] or its branched cover [4] for producing a flat metric, thus, a parameterization. Unfortunately, both the metric and the map by such a method could be non-conformal. With regard to this, using two *conjugate* harmonic one-forms (holomorphic one-forms) in [5] can produce a flat metric conformal to the original metric and conformal parameterization. However, the flat metrics induced from holomorphic one-form has only $2g-2$ (g is the genus of the mesh) cones, each of which has the angle deficit of -2π.

In this paper, we propose to use *holomorphic quadratic differentials* [6] to obtain a flat metric conformal to the original metric, thus, conformal parameterizations. As the set of holomorphic quadratic differentials is a superset of holomorphic differential one-forms, our flat metrics can be generalized to have $4g-4$ cones, each of which has the angle deficit of $-\pi$. This provides a bigger solution space than using holomorphic one-form for global parameterization. A holomorphic quadratic differential induces two harmonic measured foliations that are perpendicular to each other, called a *horizontal harmonic measured foliation* and a *vertical harmonic measured foliation*, by which the u-coordinate and the v-coordinate for parameterization can be extracted respectively. Here, by definition, it is required that the harmonic measured foliations are without poles. With regard to this, we follow the Gortler-Thurston-Palmer's algorithm [7], [8] to obtain the horizontal foliation, and develop a novel diffusion algorithm to avoid poles, which are emerged with the Gortler-Thurston-Palmer's algorithm, due to its diffusion procedure. After that, we design a method to approximate the natural coordinates of holomorphic quadratic differential.

Contributions. We summarize our contributions as follows: 1) We propose a novel geometric object called *foliation graph*, and use it to design a three-step diffusion algorithm to compute harmonic foliations without extra *poles*, which could emerge in the algorithm [8]. 2) Given only a discrete *harmonic* measured foliation, we propose an algorithm to compute the *discrete natural coordinate* of the implied holomorphic quadratic differential. 3) We apply *discrete natural coordinates* to produce *global conformal* parameterizations for high-genus meshes.

1.1 Algorithm Overview

Based on the following derivations: 1) a harmonic measured foliation induces a unique quadratic differential; 2) a holomorphic quadratic differential produces a special *natural coordinate*; 3) this *natural coordinate* corresponds to a flat metric conformal to the original metric; 4) a flat metric breeds a plane parameterization; and 5) the holomorphic maps are conformal everywhere; we design an algorithm to compute global conformal parameterizations via the natural coordinates of holomorphic quadratic differentials. The input to our algorithm is a set of loops and the corresponding

• *H. Zhao, S. Wang, and W. Wang are with the State Key Laboratory of Computer Science, Institute of Software, Chinese Academy of Sciences and the University of Chinese Academy of Sciences, Beijing, China. E-mail: {huizhao, wangsd, whn}@ios.ac.cn. corresponding author: Wencheng Wang*

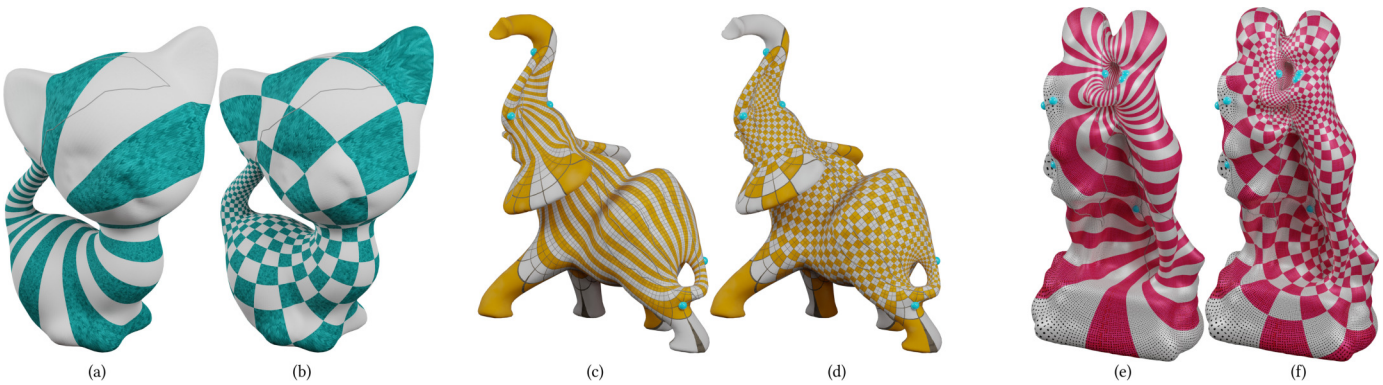

Fig. 1. The pole-free harmonic foliations (a, c, e) and holomorphic quadratic differentials (b, d, f) produced by our algorithm.

positive values on them. First, we compute a discrete pole-free harmonic foliation, which is our u-coordinate, then we calculate its counterpart v-coordinate via a dual mesh. The outputs of our method are the uv-coordinates for all vertices.

2 Related Work

Surface parameterization is a very broad topic in geometry processing. For disk-type meshes, parameterization algorithms are well explored. We refer the readers to [9] for an introduction. Here, we focus on the most relevant ones, especially parameterizations for high-genus meshes.

Crane [1] summarizes a majority of conformal algorithms for disk-type meshes as follows: 1) triangle angle preservation in the least-squares sense [10], [11]; 2) the *Cauchy-Riemann* equation preservation [12]; 3) critical points of Dirichlet energy [13]; 4) Hodge star preservation [14]; 5) conjugate harmonic functions [15]. Each of the above approaches proposes a different and non-equivalent discrete conformal structure. However, these structures only work on disk-type meshes.

Injective algorithms are proposed in [16], [17], [18], [19], [20], [21]. Nonetheless, these methods require cutting meshes into disks as a pre-process and the mapping results are not conformal. For some specific genus and configuration of cones, orbifold approaches [22], [23] can be applied to obtain injective mapping. But they are not available for arbitrary genus.

Ricci flow [24] and Calabi flow [25] can work on uncut meshes of high genus by evolving the original discrete metric (edge length) to a flat metric conformal to the original metric. However, these metric-flow based methods need an extra embedding step to achieve the mapping, which could produce numerically unstable results. Recently, Zhao et al. [26] proposes a *unit normal flow* for mesh parameterization, but their method cannot process high-genus meshes after all.

The above approaches can be classified into two methodologies: 1) the first class takes the mapping coordinates (u, v) as the unknown variables and computes them directly and simultaneously; 2) the second class computes the edge length as the first step and then the parameterization is induced from that metric.

In contrast, the following algorithms fall into the third methodology which computes the two coordinate variables u and v indirectly by integrating a global differential one-form.

Conformal parameterization from a *global* view is pioneered by Gu and Yau [5], who propose an algorithm to compute the bases of the harmonic differential one-forms. Then a conjugate counterpart of any harmonic one-form is calculated via the bases. Tong et al. [27] present a variation of Gu-Yau's algorithm by diffusing a *harmonic* one-form from a *closed* one-form. Gortler et al. [3] prove and analyze the local injectivity of the mapping results from integrating two independent harmonic one-forms by an index-counting mechanism. This is further generalized to harmonic one-forms on branched covers of high genus meshes in [4]. However, the method in [4] is not conformal and robust on high-genus meshes.

A differential one-form is discretized in [5] as real values on half-edges. Gortler and Thurston [7] defines a discrete foliation as positive values on edges. Palmer [8] derives a remarkable discrete *Whitehead* operation on foliations, which tries to smooth the values on input loop edges to the whole surfaces inside the same *Whitehead class* of foliations. Based on the work of [28], a discrete Dirichlet energy is proposed in [7], [8]. Then a diffusion method is applied in [8] to morph a discrete *closed* foliation to a discrete *harmonic* foliation via a sequence of *Whitehead* operations that decrease the energy. However, this method could generate extra poles which prevents its usage in holomorphic differentials. Based on the theoretical work of [7], [8], we develop a novel method in this paper to avoid pole emergence in [8] for producing harmonic results.

Based on graph harmonic maps [29], Lei et al. [30], [31] propose an algorithm to compute discrete holomorphic quadratic differentials, thus measured foliations. Their method works by cutting a mesh into several cylinders, then the differential one-forms computed on these cylinders are gathered together to form a holomorphic quadratic differential. While this algorithm is theoretically solid, it changes the connectivity of meshes by cutting them into cylinders across triangle faces.

A discrete foliation method is proposed in [32] to achieve bijective maps, however, it works only for simply-connected surfaces and volumes. Cohen and Ben-Chen [33] design a

flow based method to generate volumetric foliations, but their approach is limited to star-like genus-zero surfaces. While geodesic foliations are explored in [34] for fabrication, their method is not oriented for parameterization.

3 MATHEMATICAL PRELIMINARY

For the sake of clarity and conciseness, here we only give an outline and short explanation of the required mathematical background to avoid distraction from our key algorithm. We refer readers to [6], [30], [31], [35], [36], [37], [38], [39] for a more solid and formal review of the definitions of the involved concepts, especially [7], [8] for the discrete harmonic measured foliation. Although the derivation is somehow intriguing, our algorithm simply boils down to manipulating values on edges. For readers who are primarily interested in the implementation, this section could be skipped.

3.1 Complex (Conformal) Structure

A 2-dimensional manifold is a topological space that is locally regarded as $\mathbb{R}^2$. It is represented by a collection of charts $\{(U_i, \phi_i)\}_{i=1}^2$ with overlapping regions. Here $\phi_i : U_i \to \mathbb{R}^2$ is a continuous bijective map from U_i to an open set $\phi_i(U_i)$. On the overlap of two charts (U_i, ϕ_i) and (U_j, ϕ_j), the *transition function* $\phi_{ij} = \phi_j \circ \phi_i^{-1} : \phi_i(U_i \cap U_i) \to \phi_j(U_j \cap U_j)$ describes a continuous bijective transformation from $\phi_i(U_i)$ to $\phi_j(U_j)$. The set of all local charts $\{(U_i, \phi_i)\}_{i=1}^2$ forms an atlas. The charts and their transition functions determine the geometric structures. Different kinds of transition functions will produce different geometric structures.

A complex function $f : \mathbb{C} \to \mathbb{C} : x + iy \mapsto u(x, y) + iv(x, y)$ is *holomorphic*, if it satisfies the following *Cauchy-Riemann* equation $u_x = v_y, u_y = -v_x$. If f is invertible and f^{-1} is also holomorphic, then f is called a *bi-holomorphic function*. If all the transition functions of an atlas $\{(U_i, \phi_i)\}_{i=1}^2$ are bi-holomorphic, then the atlas is called a *complex atlas*. The maximal complex atlas is called a *complex structure*. A surface with a complex structure is called a *Riemann surface* [39]. For Riemann surfaces, a complex structure is also a conformal structure.

3.2 Differential One-Form

On a Riemann surface R with a complex atlas $\{(U_\alpha, \phi_\alpha)\}$, a complex-valued differential one-form $\omega : TR \to \mathbb{C}$ maps any tangent vector $v \in TR$ and scalar $\lambda \in \mathbb{C}$ to a complex $\mathbb{C}$ [8], so that:

$$\omega(\lambda v) = \lambda \omega(v).$$

Locally, ω is defined by a family $\{(U_\alpha, \phi_\alpha, \omega_\alpha)\}$, such that on each local chart with the local complex parameter z_α, there is $\omega_\alpha = \omega_\alpha(z_\alpha)dz_\alpha$. On the overlap $U_\alpha \cap U_\beta$ of two charts, $z_\alpha = \phi_{\alpha\beta}(z_\beta)$ is coordinate transformation, then coefficient function ω_α changes according to the rule: $\omega_\alpha(z_\alpha)\frac{dz_\alpha}{dz_\beta} = \omega_\beta(z_\beta)$. If $\omega_\alpha(z_\alpha)$ is a holomorphic function on every chart, ω is called as *holomorphic differential one-form*. If $\omega_\alpha(p) = 0$ at a point p on a surface R, the point p is called a *zero* point of ω, which does not change with charts.

3.3 Quadratic Differential

Differential one-form ω maps any tangent vector to a value *linearly*, yet quadratic differential $\Omega : TR \to \mathbb{C}$ *quadratically* maps any tangent vector λv [8] as:

$$\Omega(\lambda v) = \lambda^2 \Omega(v).$$

Quadratic differentials can be regarded as "*locally* the square of differential one-form". On a Riemann surface R and a coordinate chart $z_\alpha : U_\alpha \subset R \to \mathbb{C}$, a quadratic differential Ω on the whole Riemann surface R, locally on U_α, can be expressed as:

$$\Omega_\alpha = \Omega_\alpha(z_\alpha)dz_\alpha^2,$$

here $\Omega_\alpha(z_\alpha)$ is a holomorphic function on every chart, and the map Ω is called *holomorphic quadratic differential*. The coefficient function $\Omega_\alpha(z_\alpha)$ changes accordingly between different coordinate charts by the following rules: $\Omega_\alpha(z_\alpha)\frac{dz_\alpha^2}{dz_\beta^2} = \Omega_\beta(z_\beta)$.

Definition 3.1 (Zero [30])**.** A point p is called a *zero* of a holomorphic quadratic differential if $\Omega_\alpha(p) = 0$. The *zeros* do not change with charts.

Definition 3.2 (Natural Coordinate [30])**.** On a simply-connected patch U_i without *zeros* inside, a well-defined holomorphic square root of Ω, or equivalently a holomorphic differential one-form, is: $\sqrt{\Omega(p)}dz$. A holomorphic function $\zeta : U_i \to \mathbb{C}$ can be computed by the path-independent integration $\zeta(p) = \int_{p_0}^{p} \sqrt{\Omega(z)}dz$ from any point p to a fixed point p_0. The function ζ is called a *natural coordinate* on U_i.

The *natural coordinate* of a quadratic differential induces a flat metric with cone angle deficit of $-\pi$ at *zeros*. Under a quadratic differential, on every point p of Riemann surface R, a vector $v \in T_pR$ is called *horizontal* if $\Omega(v)$ is real and positive. Away from *zeros*, the pullback of the positive real axis by Ω is a line (instead of a vector). The curves, whose tangent vectors are horizontal, are the *horizontal trajectories* of Ω. The curves of the vertical (horizontal) trajectories have constant real (imaginary) natural coordinates. The trajectories through the *zeros* are called the *critical trajectories*.

3.4 Measured Foliation

Foliation [40] looks like stripe patterns on a surface (Fig. 1). A *leaf* is just a smooth line on surfaces. A measure μ can be assigned to a foliation $\mathcal{F}$ and it denotes the number of leaves that a transverse arc γ crosses. A measured foliation $|dv|$ or $((\mathcal{F}, \mu))$ [35] is defined by the real valued functions v_i defined on U_i under a set of conditions.

Definition 3.3 (Whitehead Move [40])**.** A Whitehead move is a morph of one foliation to another, consisting of three cases: 1) isotopic; 2) collapsing a finite arc between two zeros; 3) splitting a zero.

Definition 3.4 (Whitehead Class [40])**.** Two measured foliations $(\mathcal{F}, \mu)$ and $(\mathcal{G}, \nu)$ are *Whitehead* equivalent if they can be transformed to each other by some Whitehead moves. All foliations are grouped into Whitehead classes by this equivalent relationship.

A holomorphic quadratic differential Ω derives a unique measured foliation within a Whitehead class $\mathcal{F}_\Omega$ (equivalently, a unique *Whitehead class*) and vice versa.

3.5 Dirichlet Energy and Harmonic Measured Foliation

By harmonic analysis [41], a harmonic differential one-form minimizes the Dirichlet energy in its cohomology class. Similarly, according to [28], there is a kind of Dirichlet energy D for a measured foliation $|dv|$, and a harmonic foliation uniquely minimizes the Dirichlet energy in its Whitehead class [28], [42].

There are some facts about measured foliations, holomorphic differential one-forms and holomorphic quadratic differentials for a genus g closed Riemann surface. 1) The dimension of the space of all harmonic one-forms is $2g$. 1) The complex dimension of the space of all holomorphic 1-forms is g. 2) A holomorphic quadratic differential on a genus-zero closed surface must be zero. 3) The complex dimension of the space of all holomorphic quadratic differentials is $3g-3$, for the genus $g>1$. 4) A holomorphic quadratic differential has $4g-4$ *zeros* counting multiplicities. 5) The local structures around a *zero* point of order one are the complex functions: $z \to z^2$ for holomorphic differential one-forms and $z \to z^{\frac{3}{2}}$ for holomorphic quadratic differentials respectively.

4 Discrete Harmonic Measured Foliation

In this section, we discuss Gortler-Thurston-Palmer's algorithm and analyze its emergence of extra *poles*. Then we introduce a novel graph structure on a mesh, called *foliation graph*, and use it to design our pole-free algorithm.

4.1 Notations

Let $\mathsf{V},\mathsf{E},\mathsf{H},\mathsf{T}$ denote the vertices, edges, half-edges, and triangles of a manifold triangle mesh. A smooth Riemann surface M is discretized as $\mathsf{M}=(\mathsf{V},\mathsf{E},\mathsf{T})$. An edge from vertex v_i to vertex v_j is specified as $\mathsf{e}_{ij}\in\mathsf{E}$; likewise, $\mathsf{t}_{ijk}\in\mathsf{T}$ denotes a triangle. The value of a function η on a vertex v_i, a edge e_{ij} and a triangle face t_{ijk} is expressed as $\eta_i,\eta_{ij},\eta_{ijk}$. The corner i of a triangle t_{ijk} is denoted by t_i^{jk} with a subscript i and a superscript jk. While the value on a corner is denoted by the same format, for instance, $\theta_i^{jk}\in\mathbb{R}$ denotes the angle at the corner t_i^{jk}.

4.2 Gortler-Thurston-Palmer's Algorithm

In this subsection, we give a brief summary of the relevant concepts and the algorithm established in [7], [8], which paves the way for our approach.

A *discrete measured foliation* is defined as $\mathcal{F}:\mathsf{E}\to\mathbb{R}_{\geq 0}$ in [8] . If on every triangle $\mathsf{t}_{ijk}\in\mathsf{T}$, the foliation value on one edge equals to the sum of the other two edges $\mathcal{F}_{ij}=\mathcal{F}_{jk}+\mathcal{F}_{ki}$, then the foliation $\mathcal{F}$ is called *closed* [7], [8]. And the corner t_k^{ij} is called a *closed* corner and marked with symbol $\bigcirc$, meanwhile the other two corners t_i^{kj} and t_j^{ik} are marked with symbol $\times$ [7], [8] (Fig. 2). The $\bigcirc$s separate the neighboring edges of a vertex into different **sectors** $\{S_1,S_2,\ldots,S_n\}$ (Fig. 2) [8]. Let S_v denote all edges abutting on the vertex v, a discrete measured foliation $\mathcal{F}$ is *coclosed* [8] if for each sector S_k at v, there is [8]:

$$\sum_{\mathsf{e}_{ij}\in S_k}\alpha_{ij}\mathcal{F}_{ij}\leq\frac{1}{2}\sum_{\mathsf{e}_{ij}\in S_\mathsf{v}}\alpha_{ij}\mathcal{F}_{ij}, \tag{1}$$

here $\alpha_{ij}=\frac{\cot\theta_{ij}+\cot\theta_{ji}}{2}$ is the well-known cotangent weight. Palmer [8] defines a *closed* and *coclosed* foliation as a discrete *harmonic* foliation [7]. The positive value per edge measures how many leaves traverse the edge.

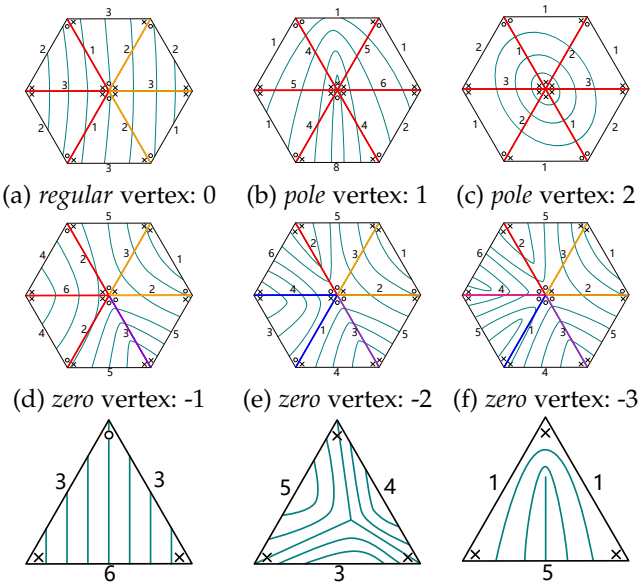

(a) *regular* vertex: 0 (b) *pole* vertex: 1 (c) *pole* vertex: 2

(d) *zero* vertex: -1 (e) *zero* vertex: -2 (f) *zero* vertex: -3

(g) *regular* triangle: 0 (h) *zero* triangle: -1 (i) *pole* triangle: 1

Fig. 2. Vertices and triangles of varying indices: the number after the colon represents the index; the edges in the same color belong to one sector. Note that the original concepts are introduced and shown in [8], while here we only provide a detailed illustration.

Let the numbers of $\bigcirc$ and $\times$ corners surrounding a vertex $\mathsf{v}\in\mathsf{V}$ be $O(\mathsf{v})$, $X(\mathsf{v})$ and the numbers inside a triangle $\mathsf{t}\in\mathsf{T}$ be $O(\mathsf{t})$, $X(\mathsf{t})$ respectively [7], [8]; let $Z(\mathsf{v})$ and $Z(\mathsf{t})$ be the number of edges whose discrete foliation value is 0 around vertex v and triangle t [7], [8]. The *index* of a vertex and a triangle are defined in [7], [8] as $i_\mathcal{F}(\mathsf{v})=2-O(\mathsf{v})+Z(\mathsf{v})$ and $i_\mathcal{F}(\mathsf{t})=2-X(\mathsf{t})-Z(\mathsf{t})$. Palmer [8] defines (Fig. 2): "For a vertex v, 1) it is *regular*, if $i_\mathcal{F}(\mathsf{v})=0$; 2) it is a *zero* of order d, if $i_\mathcal{F}(\mathsf{v})=-d$; 3) it is a *pole* of order d, if $i_\mathcal{F}(\mathsf{v})=+d$. For a triangle t; 4) it is regular, if $i_\mathcal{F}(\mathsf{t})=0$; 5) it is a *zero* of order 1, if foliation values on the three edges are all 0 or satisfy the strict triangle inequality condition; 6) it is a *pole*, if the discrete foliation value on one edge is bigger than the sum of the discrete foliation values on the other two edges."

Palmer [8] presents a remarkable *Whitehead class*-preserving *discrete Whitehead move* to evolve a foliation $\mathcal{F}$ to another $W_k\mathcal{F}$. This operation changes the values of one ring of neighboring edges of a vertex by dividing all the edges into several sectors, then adding one optimal value to each edge of some sectors and subtracting the same value from other sectors [8].

Given a set of disjoint, nontrivial triangle loops $\{L_1,L_2,\ldots,L_k\}$ and the positive values $\{w_1,w_2,\ldots,w_k\}$ on these loops, Gortler and Thurston [7] propose to create an initial *closed* foliation $\mathcal{F}(0)$ by assigning $\mathcal{F}_{ij}(0)=w_i$ to

the shared edges $\{e_{ij}\}$ of the loop L_i, and 0 to all other edges of a mesh. Then outlined in [7] and detailed in [8], a simple diffusion procedure is proposed to evolve the *closed* foliation $\mathcal{F}(0)$ to a *harmonic* foliation $\mathcal{F}(h)$ by a sequence of optimal *discrete Whitehead moves* that can decrease Dirichlet energy $\sum_{e_{ij}\in E}\alpha_{ij}\mathcal{F}_{ij}^2$ [8, Chapter 4.2]. The diffusion of their algorithm is illustrated in Fig. 3

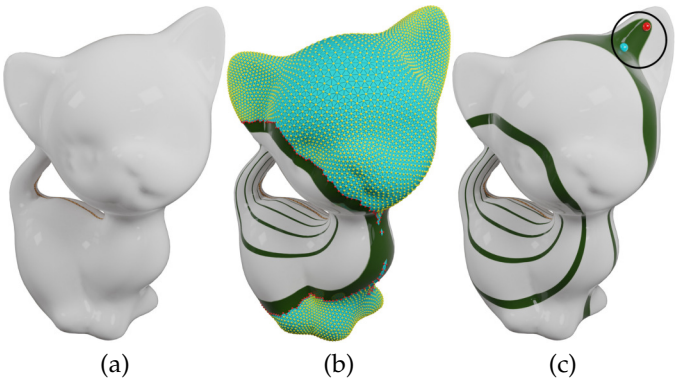

Fig. 3. The diffusion of Gortler-Thurston-Palmer's algorithm [7], [8]: (a) an input loop generating an initial *closed* foliation; (b) the *closed*, but not yet harmonic foliation (blue points are to be visited); (c) the convergent, but non-harmonic foliation with an extra *pole* (red) and *zero* (blue).

4.3 Extra Poles by Gortler-Thurston-Palmer's Algorithm

Generally speaking, all leaves of the initial foliation pass through the input triangle loops, and the optimization process should diffuse them onto the whole surface as smooth as possible, i.e., being *coclosed*. Meanwhile a *harmonic* foliation should not have any *pole*. However, the basic diffusion scheme in [8] could create extra *poles* (Fig. 3, 12, 31) and extra *zeros*. This will cause the optimization to be trapped in a local minimum. The reason is that their method does not control the diffusion procedure and the topological disk patch with its index sum bigger than 0 could emerge in their diffusion [8]. As illustrated in Fig. 4, the index sum of a topological disk patch is not 0, so that the patch will produce a *zero* or a *pole* (Fig. 4). This means that the order of traversal in diffusion does matter.

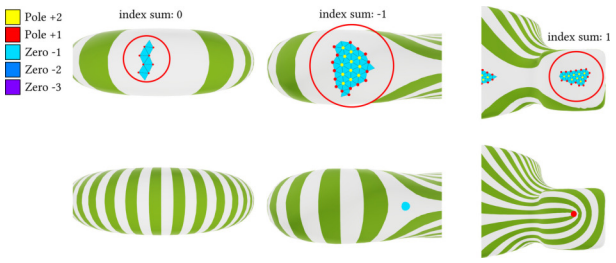

Fig. 4. Three topological disk patches with different index sums (top row) and the corresponding converged results (bottom row). The colors for singularities (both faces and vertices) of different indices are shown in the legend, which is used throughout this paper.

4.4 Foliation Graph

For a set of input loops on a mesh, we propose a novel geometric object called *foliation graph*. Different input loops will create different foliation graphs (Fig. 5).

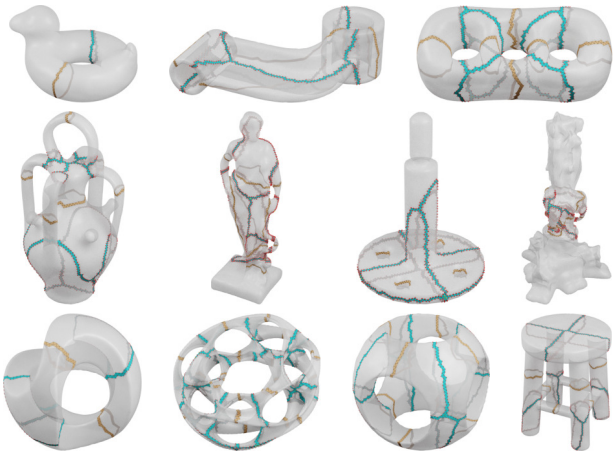

Fig. 5. The input loops (orange) and the corresponding foliation graphs (blue).

A foliation graph has two kinds of components (Fig. 6): strips of one-triangle width and junctions. The junctions have two variants: *vertex junction* or *triangle junction*, according to their connected stripes intersected at a vertex or a triangle. (Fig. 10). A strip connects two junctions (or self connecting) by intersecting at a vertex or a triangle.

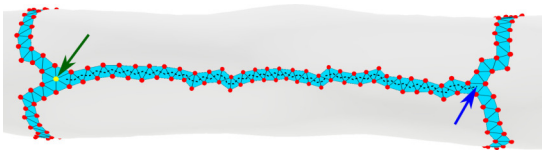

Fig. 6. The graph structure of a foliation graph: vertex junction (left green arrow), triangle junction (right blue arrow) and a strip (dotted lines in the middle) on the mesh.

The foliation graph is homotopic to the input loop on a mesh of genus one and homotopic to the critical trajectories of a foliation on high genus meshes (Fig. 5). The foliation graphs produced by homotopic input loops are homotopic as well regardless of initial weights (Fig. 7). On the other hand, homotopically nonequivalent loops will produce different foliation graphs (Fig. 8).

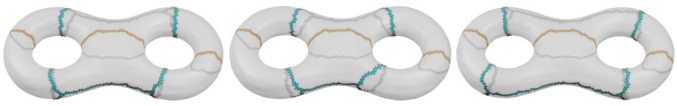

Fig. 7. The foliation graphs (blue) produced from the same input loops (orange) with different weights on a mesh are different but homotopic to each other.

The algorithm of our foliation graph generation is a variation of the breadth-first traversal. We start from the vertices in the input loops, then diffuse the edge values around them by *discrete Whitehead moves* to other triangles' edges. In our diffusion, we try to keep some triangles untouched to avoid

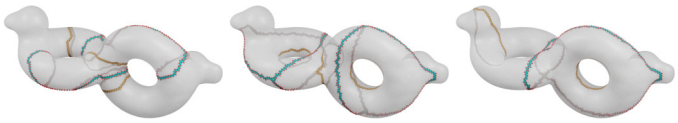

Fig. 8. The foliation graphs (blue) produced from different input loops (orange) on a mesh are different to each other.

unvisited triangles forming a topological disk. Initially, all vertices are *poles*. Then a *Whitehead* move always changes a *pole* vertex into a *regular* one [8], but the index types of its neighboring vertices remain unchanged. However, in one special situation, the neighbors may have their types changed to *regular* vertices too. We call this special *Whitehead* move as a *critical move*.

Definition 4.1 (Critical Move)**.** A *Whitehead* move is called a *critical move* if it turns any neighboring vertex from a *pole* to a *regular* vertex.

A *critical move* will cut open the strip of a foliation graph and change its topology, as shown in Fig. 9.

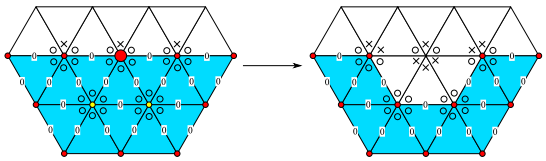

(a) Noncritical move.

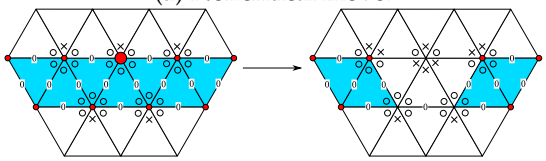

(b) Critical move.

Fig. 9. (a) A noncritical *Whitehead* move will turn the central vertex from pole to regular and keep the index type of neighboring vertices unchanged. (b) A critical move on the central vertex will remove three pole vertices and zero faces simultaneously, and cut open the foliation graph.

Definition 4.2 (Foliation Graph)**.** The vertices and faces form a *foliation graph* if any *Whitehead* move on them is a *critical move*.

The whole process is detailed in Algorithm 1, where we use a maximum heap to accelerate the diffusion process. Note that our proposed foliation graph is not the same as the well-known cut graph of a surface.

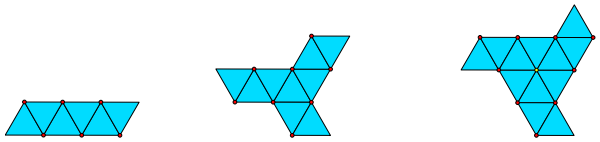

(a) a strip (b) triangle junction (c) vertex junction

Fig. 10. Whitehead moves inside a foliation graph could lead unvisited elements to form three patterns. The index sums of (a), (b) and (c) are 0, -1 and -1 respectively. None of them could produce poles.

If we perform a *critical move* inside a foliation graph, it will start to break into three kinds of topological disk patches (Fig. 10). Fortunately, no poles are created in each kind of them, as proved in the following.

Algorithm 1 Foliation Graph Generation

Input: An initial closed foliation $\mathcal{F}(0)$ on a mesh M.
Output: A Whitehead-equivalent foliation where unvisited faces form a foliation graph.

Build max heap H of vertices with energy' gradients as keys
while not all unvisited vertices are marked non-movable **do**
  $v \leftarrow H$.pop()
  attempt $\leftarrow$ WhiteheadMove(v)
  if attempt is not critical move **then**
    Perform WhiteheadMove(v)
    H.update(v, energy' gradient(v))
    for $v_i \in$ one-ring neighbor of v **do**
      H.update(v_i, energy' gradient(v_i))
      Unmark v_i
    end for
  else
    Do not perform WhiteheadMove(v)
    H.update(v, 0)
    Mark v as non-movable
  end if
end while
(*Discrete Whitehead move and energy's gradient follows [8, Chapter 4.2])

Lemma 4.1. *The diffusion of the* Whitehead *moves inside a foliation graph is pole-free.*

Proof. 1) A critical move will break up the strip of a foliation graph, where three *pole* vertices and *zero* faces will cancel each other out, as mentioned in Fig. 9. If we continue to move the tip of the strip, a zero face and pole vertex will evolve into regular elements simultaneously, so no poles or zeros are created either.

2) When a strip is disconnected from the foliation graph, as illustrated in Fig. 10(a), there are N faces and $N+2$ vertices on a triangle strip and both tip vertices on the strip are regular, thus, the index sum of this patch is guaranteed to be zero. In this case, no zeros or poles could show up.

3) Moreover, if a junction emerges in a traversal, its index sum are negative since there are N zero faces and less than N pole vertices inside them. For a triangle junction (Fig. 10(b)), any *Whitehead* move will turn (b) into one or several (a)s depending on which vertex is moved. For a vertex junction (Fig. 10(c)), this patch will degenerate to (a) or (b) after *Whitehead* moves. In either case, no poles are created and eventually, only $4g-4$ zeros are left when all elements are visited by the diffusion process.

Practically speaking, the intersection of junctions could become more complicated (Fig. 5) due to various combination of (b)s and (c)s. However, they will all degenerate to the cases described above so that we conclude that the traversal of a foliation graph is pole-free. □

4.5 Our Three-Step Diffusion Algorithm

We present a three-step diffusion algorithm (Alg. 2) for generating harmonic foliation without poles. 1) We diffuse the initial foliation to the rest of the surface by minimizing the Dirichlet energy as the same as in [8]. However, our traversal is constrained to avoid producing topological disk unvisited patches such as those in Fig. 4. In the end, the traversal of the first step will produce a foliation graph. 2) We start the diffusion inside the foliation graph. Given the special structure of the foliation graph, no extra poles could be generated in this step, as shown in the previous subsection. 3) Finally, we diffuse the yet-to-be harmonic foliation freely until the energy converges.

Algorithm 2 Three-Step Convergent Harmonic Foliation

Input: An initial closed foliation $\mathcal{F}(0)$ on a mesh M.
Output: A *Whitehead-equivalent* harmonic foliation.
1: Perform Alg.1 and get a foliation graph
2: Perform *Whitehead* moves on the vertices in the foliation graph
3: Perform *Whitehead* moves until the Dirichlet energy converges.

The key ideas in our solution are: 1) in the first step, there is no unvisited topological disk patch in diffusion; 2) the index sum of every unvisited topological disk patch in the second step is non-positive.

During the first step of our method, the $4g-4$ zeros remain inside the foliation graph, and no poles or zeros are created among the visited mesh elements outside of the foliation graph. After finishing the traversal of the first step, all vertices and triangles outside of a foliation graph are visited.

In the second step, we have argued in the Lemma 4.1 that no extra poles or zeros will emerge and there will only be $4g-4$ zeros in the foliation.

In the third step, we optimize the foliation on the whole mesh without any constraint. This step only decreases the Dirichlet energy to make foliation smoother and does not create new *poles* or *zeros*. In this step, the position of a *zero* might change depending on the energy, and it could move between face and vertex following a *Whitehead* move.

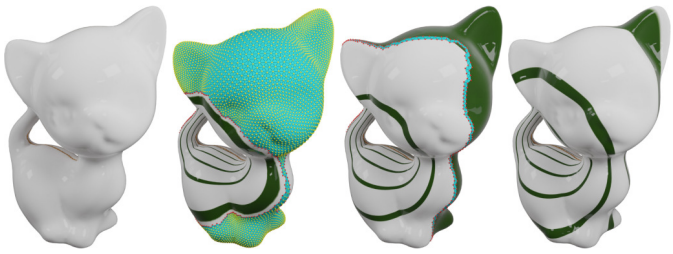

(a) (b) (c) (d)

Fig. 11. The workflow of our three-step method: (a) an input loop identical to Fig. 3; (b) minimizing the Dirichlet energy in a constrained manner in the first step; (c) a foliation-graph is formed after the completion of first step; (d) the final harmonic foliation without poles.

Our method is guaranteed to produce harmonic foliations, while the naive traversal [8] fails in a lot of configurations. We show the workflow of our algorithm in Fig 11 and compared our algorithm against the method in [8] in Fig 12. More experimental results can be found in Fig. 31. Our diffusion scheme is crucial to the construction of discrete holomorphic quadratic differentials, thus conformal parameterizations. As a *harmonic* measured foliation determines a holomorphic quadratic differential uniquely, if a foliation is not *harmonic*, its corresponding holomorphic quadratic differential cannot be computed.

5 Discretization of Holomorphic Quadratic Differential

5.1 Definitions

A *differential one-form* is discretized as real values on half-edges in [3], [5], [37]. *Holomorphic differential one-form* is discretized as complex values on half-edges in [5]. *Measured foliation* and *quadratic differential* are both discretized as positive real values on edges (not half-edges) in [7], [8].

Following the line of the above approaches, we propose to discretize a *quadratic differential* as complex values on edges of a mesh. Unlike the discretization proposed by Gortler and Thurston [7], who use discrete harmonic measured foliation directly as discrete quadratic differential (as theoretically they induce each other), we propose to use a pair of discrete harmonic measured foliations as the discretization of a quadratic differential. This subtle but crucial difference makes our discretization applicable to practical applications.

A quadratic differential induces a horizontal harmonic measured foliation and a vertical harmonic measured foliation [6]. A horizontal measured foliation uniquely determines a quadratic differential as well [35]. Hence, a horizontal measured foliation can produce a unique vertical measured foliation. Roughly speaking, the vertical foliation is a horizontal foliation rotated by 90 degree. After computing a discrete horizontal harmonic measured foliation by our three-step diffusion method, we design an algorithm to approximate its vertical counterpart indirectly via its natural coordinate.

Definition 5.1 (Discrete Holomorphic Quadratic Differential)**.** Let $\mathcal{F}$ represents a discrete horizontal harmonic measured foliation on a triangulated mesh M, and $\mathcal{F}^c$ represents its vertical counterpart, a discrete quadratic differential Q is defined as a pair of $Q(\mathcal{F},\mathcal{F}^c)$ on the primal mesh M. On every edge e, it is a complex value $Q_e(\mathcal{F}_e+\mathrm{i}\,\mathcal{F}^c_e)$.

Definition 5.2 (Foliation Cut-Graph)**.** A mesh M of genus g can be cut into a disk patch by a basic cut-graph G_b with the basis of $2g$ homotopy loops γ_h [43]. We extend G_b to a larger cut-graph G by linking all *zero* vertices of a foliation $\mathcal{F}$ to the basic cut-graph (Fig. 13). We call G as the *foliation cut-graph* of $\mathcal{F}$, which cuts M into a disk mesh M^c.

Note that foliation cut-graph is not the same as the foliation graph proposed in Sec. 4.4.

Originally, foliation values are defined on the uncut mesh. Then, we transfer them onto the cut mesh and call it the *twin foliation*.

Definition 5.3 (Twin Foliation on M^c)**.** A twin foliation $\mathcal{F}'$ on M^c is generated from $\mathcal{F}$ by replicating the foliation values $\mathcal{F}_e$ on edges e of the cut-graph G onto the twin edges e^1, e^2

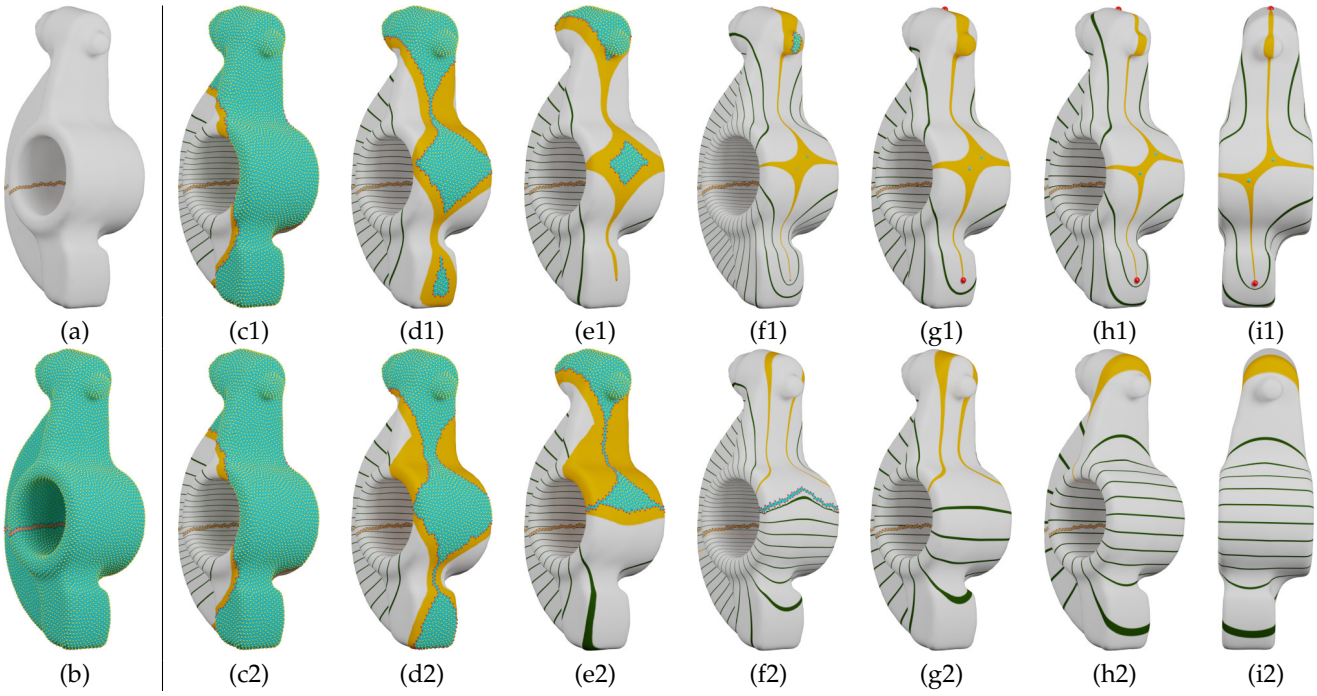

Fig. 12. The diffusion in [8] compared to our algorithm. (a) Both methods use the same input. (b) Initially, the foliation is contained within the loops while all other edges are zero-valued. However, (c1) - (i1) by [8] creates extra poles (red points) and zeros (blue points). Our algorithm avoid forming topological disks of unvisited patches in the first step (c2) - (e2). The foliation graph is formed when the first stage ends in (f2). The diffusion inside the foliation graph on the second stage eliminates the unvisited elements (g2). A pole-free harmonic foliation is generated when the energy converges (h2) - (i2).

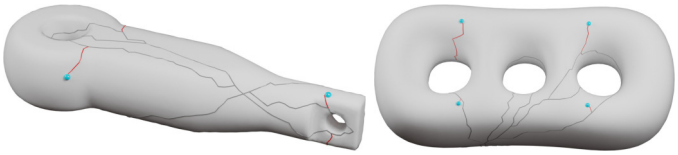

Fig. 13. Red lines connect zeros to the basic cut graph (gray lines) to form the foliation cut-graph. Natural coordinates are defined on the disk-type mesh cut by this foliation cut-graph.

of M^c. Accordingly the twin foliation $\mathcal{F}^{c'}$ on M^c is generated from $\mathcal{F}^c$.

5.2 Discrete Natural Coordinate

Definition 5.4 (Discrete Natural Coordinate)**.** Given a discrete holomorphic differential $Q(\mathcal{F}, \mathcal{F}^c)$ on mesh M, for any disk mesh M^c with *zeros* on its boundary, the complex function $(u + \mathrm{i}\, v)$ is called the *discrete natural coordinate* of the discrete holomorphic quadratic differential on M^c.

We propose to use the *discrete natural coordinate* as the parameterization coordinates. Natural coordinates corresponds to a flat metric with cones conformal to the original metric (du, dv) with cones at *zeros* [6], therefore our parameterization is conformal. Foliation $\mathcal{F}$ in our method is computed before the foliation cut-graph, and the parameterizations is the same up to translation.

5.3 Computation of the u-Coordinate

While a quadratic differential is not integrable on a closed surface, it can be turned into an integrable differential one-form on a disk patch [6], [35]. Similarly, a *closed* discrete measured foliation $\mathcal{F}$ on M can also be turned into an integrable discrete differential one-form $du : \mathsf{H} \to \mathbb{R}$ on M^c by assigning $du_{h1} = +\mathcal{F}'_e, du_{h2} = -\mathcal{F}'_e$ to the two half-edges $h1, h2$ of an edge e [8]. A function $u : \mathsf{V} \to \mathbb{R}$ on the vertices of M^c can be computed by integrating du [8].

Note that around a *zero* vertex of odd order, there is no consistent signs [8] (one positive, one negative) for each pair of twin half-edges (Fig. 14). Thus, the foliation cut-graph must pass through *zeros*.

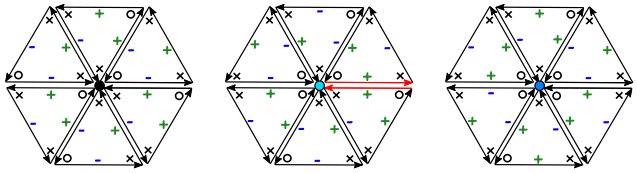

Fig. 14. The signs around (a) a *regular* vertex; (b) a *zero* vertex of odd order; (c) a *zero* vertex of even order. In the second case, the signs of half-edges couldn't be resolved consistently [8].

The *zeros* of the vertical foliation should be also located at the same vertices as the *zeros* of the horizontal foliation, as they belong to the same holomorphic quadratic differential. Thus we fix the identical zeros, and then compute the v-coordinate, as discussed in the following subsections.

5.4 Identical Zeros

On smooth surfaces, normally, the *zeros* of different harmonic foliations are located on different positions. However, a harmonic foliation and its conjugate come from the same

holomorphic quadratic differential, so their *zeros* should have identical positions.

The discrete *zeros* of a discrete harmonic foliation $\mathcal{F}$ could be on a triangle (Fig. 2h) or a vertex (Fig. 2d). If a *zero* falls on a triangle, the triangle can be divided into three sub-triangles [8], such that the *zero* appears on the newly added vertex inside the triangle and each sub-triangle is *regular* [8], as shown in Fig. 15a. As a result, we could convert all zeros on M to vertices.

Since a *zero* vertex of $\mathcal{F}$ on M corresponds to a *zero* dual face of $\widetilde{\mathcal{F}}^c$ on the dual mesh $\widetilde{\mathsf{M}}$, we propose a method to subdivide the dual faces and $\widetilde{\mathcal{F}}^c$, such that the *zeros* of $\widetilde{\mathcal{F}}^c$ fall exactly onto the same primal vertices as the *zeros* of $\mathcal{F}$. A *zero* primal vertex of index -1 has three sectors $\{S_1, S_2, S_3\}$ (Fig. 2). Then the edges on the dual face can also be divided into $\{\widetilde{S}_1, \widetilde{S}_2, \widetilde{S}_3\}$ sectors. Denote the sums of foliation values in these sectors as $\{\widetilde{\mathcal{F}}^c(\widetilde{S}_1), \widetilde{\mathcal{F}}^c(\widetilde{S}_2), \widetilde{\mathcal{F}}^c(\widetilde{S}_3)\}$. Based on Eqn. 1, they satisfy the following *coclosed* condition.

$$\begin{aligned}
\widetilde{\mathcal{F}}^c(\widetilde{S}_1) &< \widetilde{\mathcal{F}}^c(\widetilde{S}_2) + \widetilde{\mathcal{F}}^c(\widetilde{S}_3),\\
\widetilde{\mathcal{F}}^c(\widetilde{S}_2) &< \widetilde{\mathcal{F}}^c(\widetilde{S}_1) + \widetilde{\mathcal{F}}^c(\widetilde{S}_3),\\
\widetilde{\mathcal{F}}^c(\widetilde{S}_3) &< \widetilde{\mathcal{F}}^c(\widetilde{S}_1) + \widetilde{\mathcal{F}}^c(\widetilde{S}_2).
\end{aligned}$$

For a dual face, we add three edges $\widetilde{e}_1, \widetilde{e}_2, \widetilde{e}_3$ by linking the dual vertices with ◯ markers to the primal vertex. This operation divides the dual face into three sub-faces, as shown in Fig. 15b. The foliation values on three new edges are computed as follows:

$$\begin{aligned}
\widetilde{\mathcal{F}}^c_{\widetilde{e}_1} &= \frac{1}{2}(\widetilde{\mathcal{F}}^c(\widetilde{S}_1) + \widetilde{\mathcal{F}}^c(\widetilde{S}_2) - \widetilde{\mathcal{F}}^c(\widetilde{S}_3));\\
\widetilde{\mathcal{F}}^c_{\widetilde{e}_1} &= \frac{1}{2}(\widetilde{\mathcal{F}}^c(\widetilde{S}_1) + \widetilde{\mathcal{F}}^c(\widetilde{S}_3) - \widetilde{\mathcal{F}}^c(\widetilde{S}_2));\\
\widetilde{\mathcal{F}}^c_{\widetilde{e}_1} &= \frac{1}{2}(\widetilde{\mathcal{F}}^c(\widetilde{S}_3) + \widetilde{\mathcal{F}}^c(\widetilde{S}_2) - \widetilde{\mathcal{F}}^c(\widetilde{S}_1)).
\end{aligned}$$

Then all these three sub-faces are *regular*, and the *zero* of $\widetilde{\mathcal{F}}^c$ falls on the primal vertex.

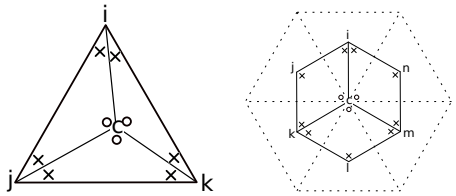

(a) (b)

Fig. 15. Both the primal zero face (a) and the dual zero face (b) could be subdivided so that the central vertex becomes a zero vertex. Note that the subdivision in (a) is introduced in [8].

5.5 Approximation of the v-Coordinate

Similarly, we'd like to convert the vertical foliation into integrable one-forms so that we could compute the v-coordinate. Note however the vertical harmonic foliation $\widetilde{\mathcal{F}}^c$ implied in [7] lives on the dual mesh $\widetilde{\mathsf{M}}$. Instead, our $\mathcal{F}^c$ is on the primal mesh M. Although the function u can be computed from $\mathcal{F}$ directly as discussed in subsection 5.3, unfortunately, $\mathcal{F}^c$ is unknown. Thus, we propose an approach to approximate the v-coordinate on the primal mesh via $\widetilde{\mathcal{F}}^c$.

We apply the discrete *Hodge star* operator [37] to compute $\widetilde{\mathcal{F}}^c$, i.e., $\widetilde{\mathcal{F}}^c_{\widetilde{ij}} = \alpha_{ij} \cdot \mathcal{F}_{ij}$ on the dual edge $\widetilde{\mathsf{e}}_{ij}$ [7]. A ◯ marker of $\mathcal{F}$ corresponds to a $\times$ marker of $\widetilde{\mathcal{F}}^c$, and vice versa (Fig. 16) [7].

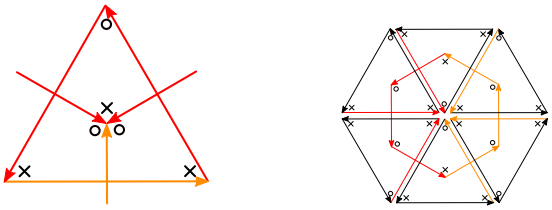

(a) primal face - dual vertex (b) primal vertex - dual face

Fig. 16. The measured foliation $\widetilde{\mathcal{F}}^c$ on the dual mesh [7], where the edges are grouped into *sectors* marked in different colors. (a) A closed primal face becomes a coclosed dual vertex. (b) A coclosed primal vertex becomes a closed dual face.

A *regular* vertex on a primal mesh has two *sectors* S_1, S_2 separated by two ◯ marker [8]. On the other hand, the foliation values of $\widetilde{\mathcal{F}}^c$ on the *regular* dual faces can be divided into two groups $\widetilde{S}_1, \widetilde{S}_2$ as well, and the sums of foliation values are equal according to the *coclosed* condition. This serves as the *closed* condition on the dual mesh (Fig. 16). Similarly, a *regular* primal triangle leads to a *regular* dual vertex. The *regular* dual vertex has two ◯ marker and one $\times$ marker, who divides the three incident edges into two *sectors* that satisfy the *coclosed* condition (Fig. 16a).

Similarly, the dual mesh $\widetilde{\mathsf{M}}$ can also be cut into a disk-topology mesh $\widetilde{\mathsf{M}}^c$ with a cut-graph $\widetilde{G}$. The foliation $\widetilde{\mathcal{F}}^{c'}$ and an exact differential one-form $d\widetilde{v} : \widetilde{\mathsf{V}} \to \mathbb{R}$ on $\widetilde{\mathsf{M}}^c$ can also be obtained from $\widetilde{\mathcal{F}}^c$. Integrating $d\widetilde{v}$, we can get a function $\widetilde{v} : \widetilde{\mathsf{V}} \to \mathbb{R}$ on the vertices of $\widetilde{\mathsf{M}}^c$, such that,

$$\widetilde{\mathcal{F}}'^c_{ij} = |\widetilde{v}_i - \widetilde{v}_j|.$$

Finally the function $v : \mathsf{V} \to \mathbb{R}$ on M^c is computed from $\widetilde{v}$. The value v_i is computed by averaging the values $\widetilde{v}_j$ on the dual vertices of the corresponding dual face.

$$v_i = \frac{1}{n}\sum_{j=1}^{n} \widetilde{v}_j \tag{2}$$

5.5.1 Extended Mesh

Note that the value v from Eqn. 2 should respect the cut graph G used by the horizontal integration. However, half of the neighboring triangles for a boundary vertex on the cut-graph are cut off. We introduce the *extended mesh* to solve this problem. An *extended mesh* M^{ce} (Fig. 18) extends the cut mesh M^c along its boundary with neighboring triangles on the other side of the cut-graph in the uncut mesh M. The whole algorithm is listed in Alg. 3 and the whole work-flow is summarized as follows:

$$\mathcal{F} \implies \widetilde{\mathcal{F}}^c \implies \widetilde{\mathcal{F}}^{c'} \implies d\widetilde{v} \implies \widetilde{v} \implies v$$

5.6 Admissible Curve System

On a surface of genus g , a set of non-intersecting, disjoint, pairwise not homotopic, homotopically nontrivial simple loops $\Gamma = \{\gamma_1, \ldots, \gamma_n\}$ $(n \leq 3g-3)$ is called an *admissible*

Fig. 17. A gallery of global conformal parameterizations produced by our method. The shapes of the texture circles are well preserved, exhibiting the conformality of our method.

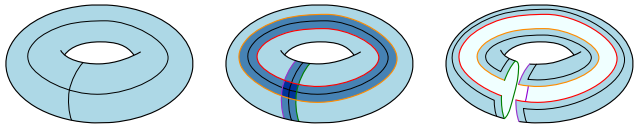

(a) (b) (c)

Fig. 18. We extend the mesh for dual integration: (a) cut the mesh along the cut graph; (b) extend the mesh beyond the borders; (c) border vertices become interior vertices so dual integration works in the same way for all vertices.

Algorithm 3 Approximation of the v-coordinate

Input: Mesh M, Foliation $\mathcal{F}$, Cut graph G
Output: the v-coordinate

Cut M into the disk mesh M^c using G
for all V_i^c on the border of M^c **do**
    $V_i \leftarrow$ identical to V_i^c on the original mesh
    Add 1-ring face of V_i to V_i^c if its counterpart is not in M^c
end for
Build the dual mesh $\widetilde{\mathsf{M}}^{ce}$ on the extended mesh M^{ce}
Compute Hodge dual $\widetilde{\mathcal{F}^c}$ and convert it to 1-forms on $\widetilde{\mathsf{M}}^{ce}$
$v^c \leftarrow$ integrate 1-forms on $\widetilde{\mathsf{M}}^{ce}$
for all V_i^c in M^c **do**
    Compute v_i from v_i^c according to Eqn. 2
end for

curve system [44, Chapter 11], as shown in Fig. 19. Two admissible curve systems Γ and $\widetilde{\Gamma}$ with the same number of loops are called compatible, if each γ_i is homotopic to $\widetilde{\gamma}_i$.

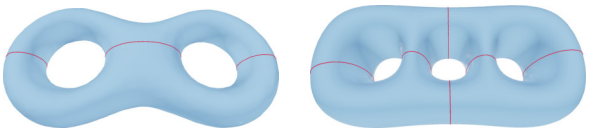

(a) $3g-3=3$ (b) $3g-3=6$

Fig. 19. Two admissible curve systems of non-intersecting simple loops for a mesh of genus 2 and 3 respectively.

Theorem 5.1 ([6]). *The maximal number n of loops in an admissible curve system on a compact Riemann surface of genus is $n=3g-3$ for $g>1$; $n=0$ for $g=0$, $n=0$; and $n=1$ for $g=1$.*

Theorem 5.2 ([30], [35]). *Given a set of admissible simple loops $\Gamma=\{\gamma_1,\ldots,\gamma_n\}$, and $n\leq 3g-3$ and positive numbers $\{w_1,\ldots,w_n\}$, there exists a unique holomorphic quadratic differential such that it has these weights as foliation values along these loops.*

These two theorems complete the story of our approach. The input to our algorithm is an admissible curve system, and the initial foliation values assigned on them correspond to $\{w_1,\ldots,w_n\}$ in theorem 5.2. The number of admissible curve systems is infinite, and every holomorphic quadratic differential (and a harmonic measured foliation) can be achieved from a certain admissible curve system. The compatible admissible curve systems induce the same holomorphic quadratic differential.

5.7 The Workflow

The cotangent weights must be positive [7]. Thus, our parameterization method requires an intrinsically Delaunay triangulation, which can be achieved by performing edge flips on any triangle mesh [45]. The intrinsic Delaunay triangulation has the same *conformal structure* (i.e., holomorphic quadratic differentials) with the original mesh (as discussed in [1, Sec. 1.5.2]). An admissible *triangle loop* is a cycle of triangles sharing one edge with its neighbors. Three automatic methods could be used to create *edge loops*: 1) the greedy homotopy basis method [43]; 2) the handle and tunnel algorithms in [46]; 3) $3g-3$ loops [30]. After that, the *triangle loops* are generated from these *edge loops* directly. We list all the steps in Algorithm 4.

6 Experiments And Demonstrations

The only required input to our parameterization is an admissible curve system which can be produced automatically and robustly. Our method is also insensitive to the exact locations of admissible curve systems as well as mesh triangulation and resolution. The whole system is automatic.

Algorithm 4 Global conformal parameterization

Input: A high-genus Delaunay triangle mesh M, Admissible input loops L

Output: A conformal, and cut-free parameterization (u, v)

1: Compute harmonic horizontal foliation $\mathcal{F}$ using Alg. 2
2: Build cut-graph G for M
3: Cut M along G to get the topological disk mesh M^c
4: Integrate $\mathcal{F}$ on G^c to get the u-coordinate
5: Use Alg. 3 to compute the v-coordinate

Below we demonstrate our algorithm in terms of these aspects and compare it with previous methods. Please refer to the supplementary videos for a more vivid illustration.

6.1 Conformal Mapping

Built on a solid theoretical ground, our parameterization method can produce *conformal* results, as shown in the gallery in Fig. 17. The conformality could be seen from the preserved circles on the surfaces.

6.2 The Number of Input Loops

According to theorem 5.1, we can have at most $3g - 3$ loops in an admissible curve system. The foliations and parameterizations generated by different numbers of loops in our algorithm are exhibited in Fig. 20.

Fig. 20. 1 to 6 ($3g - 3$) input loops. The top row shows the horizontal foliation and the bottom row shows the conformal parameterization.

6.3 Using All Handle and Tunnel Loops

In practice, we do not need to choose the input loops manually. We can use all handle loops or tunnel loops automatically generated by [46] for nice quality parameterizations, as shown in Fig. 21

6.4 Discussion on Conjugacy

A straightforward attempt is trying to use a handle loop [46] for the horizontal foliation, and its corresponding tunnel loop for the vertical foliation. However, these two foliations cannot induce a holomorphic quadratic differential, i.e., a conformal parameterization, as demonstrated in Fig. 22.

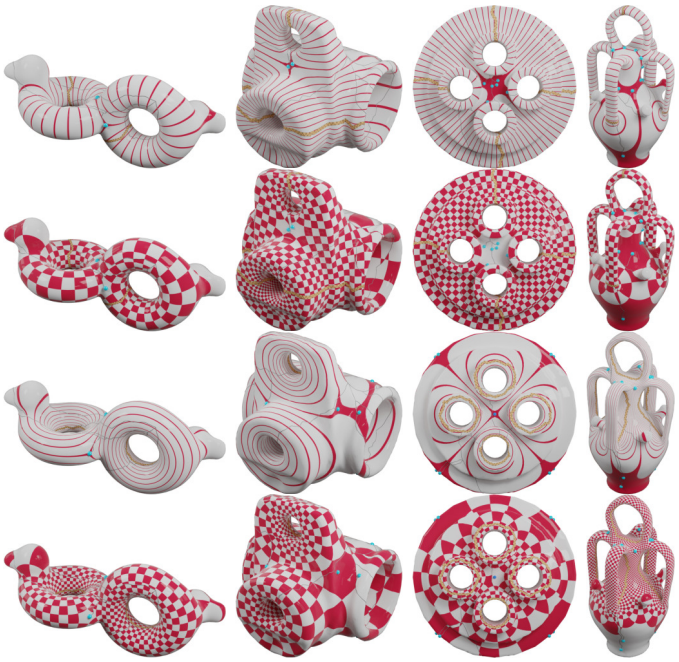

Fig. 21. The foliations and parameterizations computed from g handle (1st, 2nd row) and tunnel (3rd, 4th row) loops of each mesh.

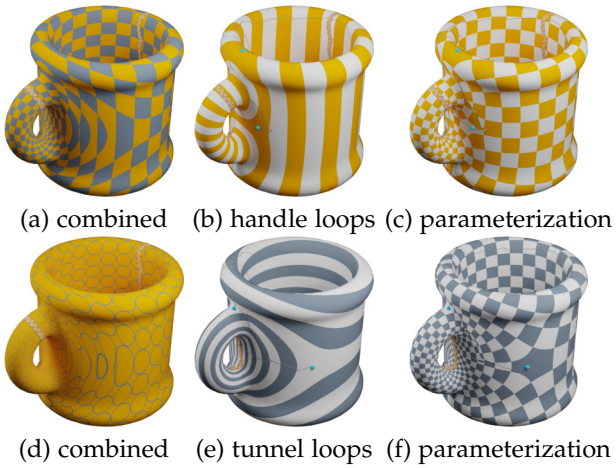

Fig. 22. The foliations are generated with all handles (b) and all tunnels (e) respectively. Their corresponding conformal parameterizations by our algorithm are exhibited in (c) and (f). However, the combination of (b) and (e) will not produce a conformal parameterization, as shown by distorted ellipses and rectangles in (a) and (d).

6.5 Homotopic Loops Convergence

Compatible admissible curve systems (i.e., homotopic loops) generate the same harmonic measured foliation [8] and holomorphic quadratic differentials, i.e., *discrete natural coordinates*. Therefore our parameterization result is robust against large variations of input loops as long as they remain homotopic, as exhibited in Fig. 23.

Our method can easily produce different parameterizations by homotopically different input loops, as shown in Fig. 24.

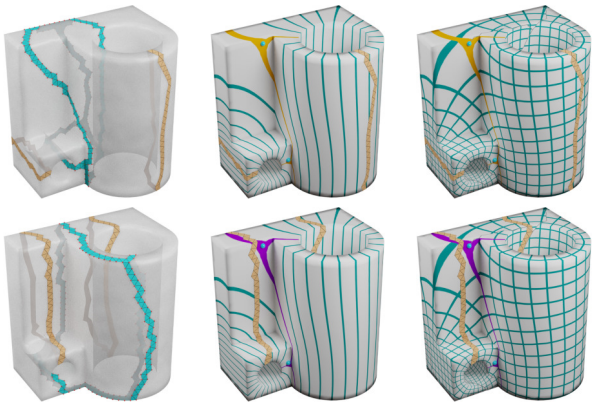

Fig. 23. The harmonic foliations (middle) and conformal parameterizations (right) are the same from different foliation graphs produced by homotopic loops (left).

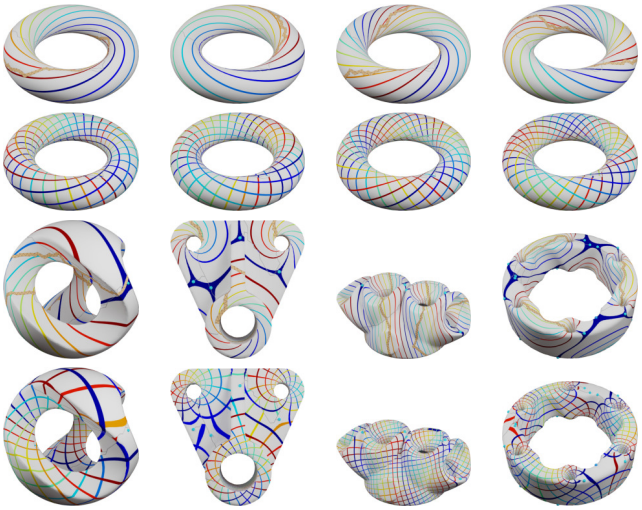

Fig. 24. Different foliations (1st, 3rd row) and parameterizations (2nd, 4th row) controlled by input loops.

6.6 Triangulation and Resolution Robustness

Our conformal results are insensitive to triangulations and resolutions, as shown in Fig. 25. This probably benefits from the used cotangent weight, which can capture the conformal structures of the meshes.

(a) (b) (c) (d)

Fig. 25. The positions of zeros in different configurations and grid lines are almost in the same places of the horse shape for the meshes of different resolutions ((a),(b): 3000 vertices; (c),(d): 27000 vertices).

6.7 Closed and Harmonic Foliations

A *harmonic* foliation is the smoothest one in its *Whitehead class* [28]. Fig. 26 shows some *closed*, but not yet *harmonic* foliations and their *harmonic* counterpart. The detailed diffusion procedures are illustrated in the supplementary video.

Fig. 26. A closed foliation gradually evolves into a harmonic one with our algorithm.

6.8 Comparison with Gortler-Thurston-Palmer's Algorithm

We compare our three-step method with Gortler-Thurston-Palmer's algorithm on dozens of commonly known meshes of high genus in the graphics community. Their method fails in plenty of cases, while ours can produce harmonic measured foliations successfully. Some results are exhibited in Fig. 31.

6.9 Comparison with holomorphic 1-forms

The most closely related parameterization algorithm to ours is built on discrete holomorphic differential one-forms [5]. Holomorphic quadratic differentials (of dim $3g-3$) generalize holomorphic differential one-forms (of dim g). Thus, our method can produce a larger space of conformal parameterizations for the same mesh of genus g. Specifically, the *zeros* of a harmonic one-form have index of -2 (Fig. 28 a1, b1, c1, d1), and -1 for foliations (Fig. 28 e, f). A close-up view of the *zeros* is exhibit in Fig. 27. The number of *zeros* in the example are $2g-2$ (holomorphic one-form) and $4g-4$ (holomorphic quadratic differentials) respectively. Therefore, the conformal parameterization of our method have less distortion, as shown in Fig. 29 and Fig. 32.

(a) (b) (c) (d)

Fig. 27. Zero of index -2 produced by harmonic 1-forms (a), (b); zero of index -1 produced by harmonic foliation (c), (d).

As harmonic one-forms are just special harmonic foliations, our method can also produce harmonic one-forms by specific input loops, as shown in Fig. 28(a3, b3). By carefully choosing the initial values for the loops, two index -1 zeros could merge into a single index -2 zero.

The approach in [5], [27] also starts from a *closed*, but not harmonic one-form according to a single input loop, then they use a linear system to compute the harmonic one. Note that using the same input loop in [5], [27] and ours are not supposed to generate the same results (the second row of Fig. 28), as these two algorithms are fundamentally different.

6.10 Convergence

In the experiments, we use an epsilon to stop the optimization procedure. If the change of the energy is less than the epsilon value, we obtain a harmonic foliation from an

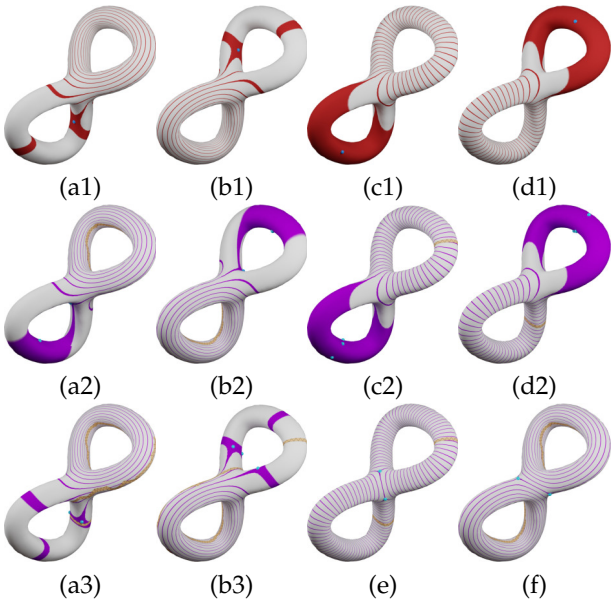

Fig. 28. [5] produces $2g$ harmonic 1-forms basis (1st row) on a mesh of genus g. Our algorithm (2nd row) uses the same input loops as for the 1st row, but (a2,b2) generate different results from (a1,b1), meanwhile (c2,d2) generate the same results as (c1,d1). (a3,b3) show that, with specified loops and initial values, our method can produce the same results with (a1,b1). Our algorithm could also produce results with *zeros* of cone angle deficit of $-\pi$, which one-forms fail to achieve (e,f).

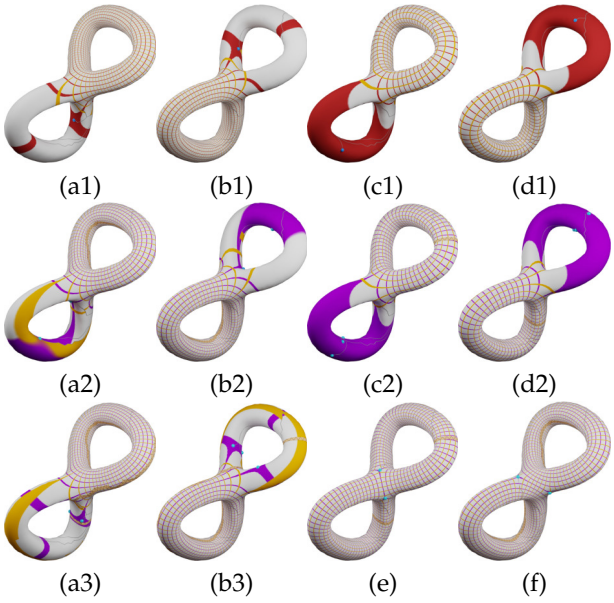

Fig. 29. Parameterizations corresponding to Fig. 28.

input *closed* foliation. The convergence time grows with the increased resolution of the mesh. Meanwhile, the computational time could also vary a lot according to the shape of the mesh as well as the input loops, even when the meshes have the same number of vertices. In our experiments, the typical convergence time ranges from a few seconds to several minutes for the meshes with 30,000 vertices or less. All the experiments were conducted on a computer with Intel Core i7-6700 CPU @ 3.40GHz and 16GB of memory. The convergence rate of some meshes are exhibited in Fig. 30. Note that our timing is almost the same as the one in [8], even though our diffusion procedure has three steps.

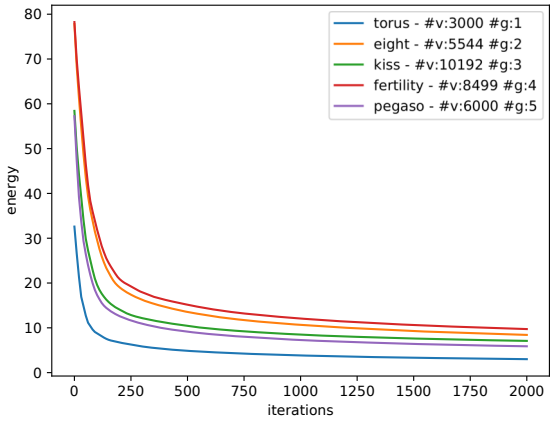

Fig. 30. The convergence rate of our diffusion procedure. The number of vertices and genus for each mesh are marked in the legend; every iteration is a single optimal Whitehead move [8, Chapter 4.2] on one vertex. The iteration unit is millions.

6.11 Limitation and Discussion

In the following, we have some discussions about our method.

Firstly, our method based on holomorphic quadratic differentials has limitation in terms of cone angle deficit of $-\pi$, but ours is a step further following holomorphic one-form in [5], whose cone angle deficit is -2π. The holomorphic quartic differentials [47] can produce results with cone angle deficit of $-\pi/2$, but there are not discrete algorithms for it on high-genus meshes by now.

Secondly, the *zeros* and *poles* correspond to the cones of the negative and positive Gaussian curvatures. A holomorphic differential has only a fixed number, $4g-4$, of *zeros* and no *poles*, while the cones of positive Gaussian curvatures are necessary to reduce the distortion in parameterization. Therefore our conformal feature is achieved by the price of producing only a flat metric with a restricted set of cones. There are not holomorphic quadratic differentials on genus-zero surfaces, therefore our approach cannot process them.

Thirdly, two paired harmonic functions can produce a local injective result [3], [4]. As for our method, it can produce a harmonic u-coordinate, but our v-coordinate is computed by an approximation, which cannot be guaranteed to be exactly harmonic. This prevents the local injectivity of our method. Even so, as our u-coordinate is exactly harmonic, in the extensive experiments, our method produces no or a few triangle flips in each test on the mesh with around dozens of thousands of triangles. The corresponding statistics are provided in the supplementary materials.

Fourthly, theoretically, the mapping results based on holomorphic quadratic differentials should be seamless, because the discrete holonomies [48] from holomorphic quadratic differentials satisfy the seamless condition [2], [49]. Unfortunately, the seamlessness is an "exact or not" property, which cannot be approximated, and so our approximated v-coordinate destroys the seamless property of the mapping. Our on-going work is to solve the approximation problem to achieve a seamless parameterization.

Fifthyly, in [47], Lei et al. proved that the positions of *zeros* of holomorphic differentials one-form, quadratic differentials, quartic differentials are not random and their positions must satisfy the so-called Abel-Jacobi condition. As a result, the positions of *zeros* (or cones) on high-genus surfaces cannot be placed freely, as these positions are determined optimally and globally. Thus, for our conformal higher-genus parameterization, the positions of cones are not freely choosable.

Sixthly, with the cotangent weight, two paired differential harmonic one-forms produce a holomorphic one-form with respect to the current metric of the mesh [5]. In some sense, if different weights are used [3], [4], then, basically, the resulting one-form [4] could also be considered as a "holomorphic" one, but with respect to another implied "metric" of the mesh. By the discussion in the last paragraph, this "holomorphic" one-form should also satisfy the Abel-Jacobi condition, but under a different metric now. Thus, we may conclude that if the positions of *zeros* (cones) are fixed on a high-genus surface, the system cannot be guaranteed to have a solution. This insolubility is already observed experimentally and pointed out in [4]: "*we noted that with higher genus models it was sometimes difficult to find good frames, and the frames from [50] would sometimes lead to infeasibility*." Of course, on a genus-zero surface, the Abel-Jacobi condition is satisfied by any positions of *zeros* [47]. Thus, the positions of *zeros* can be fixed in advance on genus-zero meshes to obtain a solution, as demonstrated in [51].

7 Conclusion

In this paper, by analyzing the reason for *pole* emergence in Gortler-Thurston-Palmer's algorithm [7], [8], we propose a practical approach to compute discrete *harmonic* measured foliations with the assistance of a novel geometric object called *foliation graph* to avoid *poles*. Then we provide a workflow to extract the *discrete natural coordinates* from a discrete *harmonic* measured foliation based on the theory of holomorphic quadratic differential. Finally, we apply *discrete natural coordinates* to create a conformal and holonomy-controllable mesh parameterizations.

Note that we do not compute the vertical harmonic foliations explicitly, but take an approximation way to obtain the v-coordinates. As far as the conformal parameterization is concerned, our mechanism works well. As a future issue, it is interesting to produce a vertical harmonic foliation in the original mesh for exactly computing v-coordinates, instead of approximating them by the dual mesh.

Currently, our diffusion step is expensive due to millions of *Whitehead* moves. It is interesting to look for an acceleration scheme for it. In the future, we would also like to explore the applications of quasi-conformal mapping and quadrangulation with the tool of discrete holomorphic quadratic differential. Considering that the conformal mapping distorts the area, the adaption of the algorithms to area-preserving parameterization for meshes of high genus is also a potentially interesting research direction.

Acknowledgements

We would like to thank anonymous reviewers for their insightful feedback, valuable comments, and suggestions. The first author would like thank Prof. Steven J. Gortler for discussion and invitation to visit Harvard and Prof. Xianfeng Gu's Lectures on the holomorphic quadratic differentials. Meshes are courtesy of the AIM@SHAPE shape repository, Thingi10K project [52], and the dataset provided by [2]. The duck model is from Keenan Crane's 3D Model Repository. This work is partially supported by the National Key R&D Program of China under Grant No.: 2017YFB1002701 and the National Natural Science Foundation of China under Grant No. 61661146002.

References

[1] K. Crane, "Conformal geometry of simplicial surfaces," 2019. [Online]. Available: http://www.cs.cmu.edu/~kmcrane/Projects/Other/ConformalGeometryOfSimplicialSurfaces.pdf

[2] A. Myles and D. Zorin, "Global parametrization by incremental flattening," *ACM Transactions on Graphics (TOG)*, vol. 31, no. 4, pp. 1–11, 2012.

[3] S. J. Gortler, C. Gotsman, and D. Thurston, "Discrete one-forms on meshes and applications to 3d mesh parameterization," *Computer Aided Geometric Design*, vol. 23, no. 2, p. 83–112, Feb. 2006.

[4] A. Bright, E. Chien, and O. Weber, "Harmonic global parametrization with rational holonomy," *ACM Transactions on Graphics (TOG)*, vol. 36, no. 4, p. 89, 2017.

[5] X. Gu and S.-T. Yau, "Global conformal surface parameterization," in *Proceedings of the 2003 Eurographics/ACM SIGGRAPH Symposium on Geometry Processing*, ser. SGP '03, 2003, p. 127–137.

[6] K. Strebel, "Quadratic differentials," in *Quadratic Differentials*. USA: Springer, 1984, pp. 16–26.

[7] S. J. Gortler and D. P. Thurston, "Discrete quadratic differentials," 2015. [Online]. Available: http://pages.iu.edu/~dpthurst/writing/discrete-qd.pdf

[8] D. Palmer, "Toward computing extremal quasiconformal maps via discrete harmonic measured foliations," Bachelor's thesis, Harvard College, Cambridge, Massachusetts, USA, 7 2015.

[9] M. S. Floater and K. Hormann, "Surface parameterization: a tutorial and survey," in *Mathematics and Visualization*. Berlin, Heidelberg: Springer-Verlag, 2005, pp. 157–186.

[10] A. Sheffer, B. Lévy, M. Mogilnitsky, and A. Bogomyakov, "Abf++: fast and robust angle based flattening," *ACM Transactions on Graphics (TOG)*, vol. 24, no. 2, pp. 311–330, 2005.

[11] R. Zayer, B. Lévy, and H.-P. Seidel, "Linear angle based parameterization," in *Proceedings of the Fifth Eurographics Symposium on Geometry Processing*, ser. SGP '07. Goslar, DEU: Eurographics Association, 2007, p. 135–141.

[12] B. Lévy, S. Petitjean, N. Ray, and J. Maillot, "Least squares conformal maps for automatic texture atlas generation," *ACM Trans. Graph.*, vol. 21, no. 3, p. 362–371, Jul. 2002.

[13] U. Pinkall and K. Polthier, "Computing discrete minimal surfaces and their conjugates," *Experimental mathematics*, vol. 2, no. 1, pp. 15–36, 1993.

[14] C. Mercat, "Discrete riemann surfaces and the ising model," *Communications in Mathematical Physics*, vol. 218, no. 1, pp. 177–216, 2001.

[15] R. Sawhney and K. Crane, "Boundary first flattening," *ACM Transactions on Graphics (TOG)*, vol. 37, no. 1, p. 5, 2017.

[16] S. Z. Kovalsky, M. Galun, and Y. Lipman, "Accelerated quadratic proxy for geometric optimization," *ACM Transactions on Graphics (TOG)*, vol. 35, no. 4, p. 134, 2016.

[17] L. Liu, C. Ye, R. Ni, and X.-M. Fu, "Progressive parameterizations," *ACM Transactions on Graphics (TOG)*, vol. 37, no. 4, p. 41, 2018.

[18] M. Rabinovich, R. Poranne, D. Panozzo, and O. Sorkine-Hornung, "Scalable locally injective mappings," *ACM Transactions on Graphics (TOG)*, vol. 36, no. 2, p. 16, 2017.

[19] C. Schüller, L. Kavan, D. Panozzo, and O. Sorkine-Hornung, "Locally injective mappings," in *Proceedings of the Eleventh Eurographics/ACMSIGGRAPH Symposium on Geometry Processing*, ser. SGP '13. Goslar, DEU: Eurographics Association, 2013, p. 125–135.

Fig. 31. Gortler-Thurston-Palmer's Algorithm [7], [8] (1st, 3rd row) compared to ours (2nd, 4th row). Note the extra poles created by their algorithm, which are represented by red spheres and have been highlighted using red circles in the top-right figure.

Fig. 32. Comparisons between holomorphic 1-forms (1st, 2nd rows) and ours (3rd, 4th rows).

[20] A. Shtengel, R. Poranne, O. Sorkine-Hornung, S. Z. Kovalsky, and Y. Lipman, "Geometric optimization via composite majorization," *ACM Trans. Graph*, vol. 36, no. 4, p. 38, 2017.

[21] Y. Zhu, R. Bridson, and D. M. Kaufman, "Blended cured quasi-newton for distortion optimization," *ACM Transactions on Graphics (TOG)*, vol. 37, no. 4, p. 40, 2018.

[22] N. Aigerman and Y. Lipman, "Orbifold tutte embeddings," *ACM Trans. Graph.*, vol. 34, no. 6, pp. 190–1, 2015.

[23] N. Aigerman, S. Z. Kovalsky, and Y. Lipman, "Spherical orbifold tutte embeddings," *ACM Transactions on Graphics (TOG)*, vol. 36, no. 4, p. 90, 2017.

[24] M. Jin, J. Kim, and X. D. Gu, "Discrete surface ricci flow: Theory and applications," in *Proceedings of the 12th IMA International Conference on Mathematics of Surfaces XII*. Berlin, Heidelberg: Springer-Verlag, 2007, p. 209–232.

[25] H. Zhao, X. Li, H. Ge, N. Lei, M. Zhang, X. Wang, and X. Gu,

"Conformal mesh parameterization using discrete calabi flow," *Computer Aided Geometric Design*, vol. 63, pp. 96–108, 2018.

[26] H. Zhao, K. Su, C. Li, B. Zhang, L. Yang, N. Lei, X. Wang, S. J. Gortler, and X. Gu, "Mesh Parametrization Driven by Unit Normal Flow," *Computer Graphics Forum*, vol. 39, no. 1, pp. 34–49, Feb. 2020. [Online]. Available: https://onlinelibrary.wiley.com/doi/abs/10.1111/cgf.13660

[27] Y. Tong, P. Alliez, D. Cohen-Steiner, and M. Desbrun, "Designing quadrangulations with discrete harmonic forms," in *Proceedings of the Fourth Eurographics Symposium on Geometry Processing*, ser. SGP '06. Goslar, DEU: Eurographics Association, 2006, p. 201–210.

[28] F. P. Gardiner and N. Lakic, "The dirichlet principle for measured foliations," 2010.

[29] M. Wolf, "On realizing measured foliations via quadratic differentials of harmonic maps to r-trees," *Journal d'Analyse Mathematique*, vol. 68, no. 1, pp. 107–120, 1996.

[30] N. Lei, X. Zheng, J. Jiang, Y.-Y. Lin, and D. X. Gu, "Quadrilateral and hexahedral mesh generation based on surface foliation theory," *Computer Methods in Applied Mechanics and Engineering*, vol. 316, pp. 758–781, 2017.

[31] N. Lei, X. Zheng, Z. Luo, and D. X. Gu, "Quadrilateral and hexahedral mesh generation based on surface foliation theory ii," *Computer Methods in Applied Mechanics and Engineering*, vol. 321, pp. 406–426, 2017.

[32] M. Campen, C. T. Silva, and D. Zorin, "Bijective maps from simplicial foliations," *ACM Transactions on Graphics (TOG)*, vol. 35, no. 4, p. 74, 2016.

[33] D. Cohen and M. Ben-Chen, "Generalized volumetric foliation from inverted viscous flow," *Computers & Graphics*, vol. 82, pp. 152–162, Aug. 2019.

[34] J. Vekhter, J. Zhuo, L. F. G. Fandino, Q. Huang, and E. Vouga, "Weaving geodesic foliations," *ACM Transactions on Graphics (TOG)*, vol. 38, no. 4, p. 34, 2019.

[35] J. Hubbard and H. Masur, "Quadratic differentials and foliations," *Acta Mathematica*, vol. 142, no. 1, pp. 221–274, 1979.

[36] W. P. Thurston and S. Levy, *Three-dimensional geometry and topology*. USA: Princeton University Press, 1997, vol. 1.

[37] K. Crane, F. de Goes, M. Desbrun, and P. Schröder, "Digital geometry processing with discrete exterior calculus," in *ACM SIGGRAPH 2013 Courses*, ser. SIGGRAPH '13. New York, NY, USA: Association for Computing Machinery, 2013.

[38] M. Fortier Bourque, "The holomorphic couch theorem," *Inventiones mathematicae*, vol. 212, no. 2, pp. 319–406, May 2018.

[39] J. Jost, *Compact Riemann Surfaces: An Introduction to Contemporary Mathematics*. Springer, aug 2006.

[40] A. Fathi, *Thurston's Work on Surfaces*. New Jersey, United States: Princeton University Press, apr 2012.

[41] R. M. Schoen and S.-T. Yau, *Lectures on harmonic maps*. USA: Amer Mathematical Society, 1997, vol. 2.

[42] F. P. Gardiner and N. Lakic, "A synopsis of the dirichlet principle for measured foliations (infinite dimensional teichmuller spaces and moduli spaces)," 2010.

[43] J. Erickson and K. Whittlesey, "Greedy optimal homotopy and homology generators," in *Proceedings of the Sixteenth Annual ACM-SIAM Symposium on Discrete Algorithms*, ser. SODA '05. USA: Society for Industrial and Applied Mathematics, 2005, p. 1038–1046.

[44] F. P. Gardiner, *Quasiconformal Teichmuller Theory*. USA: American Mathematical Society, dec 1999.

[45] M. Fisher, B. Springborn, P. Schröder, and A. I. Bobenko, "An algorithm for the construction of intrinsic delaunay triangulations with applications to digital geometry processing," *Computing*, vol. 81, no. 2-3, pp. 199–213, 2007.

[46] T. K. Dey, F. Fan, and Y. Wang, "An efficient computation of handle and tunnel loops via reeb graphs," *ACM Transactions on Graphics (TOG)*, vol. 32, no. 4, p. 32, 2013.

[47] N. Lei, X. Zheng, Z. Luo, F. Luo, and X. Gu, "Quadrilateral mesh generation II: Meromorphic quartic differentials and Abel–Jacobi condition," *Computer Methods in Applied Mechanics and Engineering*, vol. 366, p. 112980, Jul. 2020.

[48] W. Chen, X. Zheng, J. Ke, N. Lei, Z. Luo, and X. Gu, "Quadrilateral mesh generation I : Metric based method," *Computer Methods in Applied Mechanics and Engineering*, vol. 356, pp. 652–668, Nov. 2019.

[49] M. Campen, H. Shen, J. Zhou, and D. Zorin, "Seamless parametrization with arbitrary cones for arbitrary genus," *ACM Transactions on Graphics (TOG)*, vol. 39, no. 1, pp. 1–19, 2019.

[50] D. Bommes, H. Zimmer, and L. Kobbelt, "Mixed-integer quadrangulation," *ACM Transactions On Graphics (TOG)*, vol. 28, no. 3, p. 77, 2009.

[51] E. F. Hefetz, E. Chien, and O. Weber, "A subspace method for fast locally injective harmonic mapping," in *Computer Graphics Forum*, vol. 38, no. 2. Wiley Online Library, 2019, pp. 105–119.

[52] Q. Zhou and A. Jacobson, "Thingi10k: A dataset of 10,000 3d-printing models," 2016.

Hui Zhao received his M.Phil. degree from Computer Science and Engineering Department at Hong Kong University of Science and Technology in 2007. He was a visiting scholar in Harvard University from 2015 to 2016. He has developed mesh processing software (MeshDGP) and published five books on computer graphics. He is currently a Ph.D. student with the State Key Laboratory of Computer Science, Institute of Software, Chinese Academy of Science.

Shaodong Wang received his B.Sc. degree from the School of Resource and Environmental Sciences at Wuhan University. He is currently a Ph.D. student with the State Key Laboratory of Computer Science, Institute of Software, Chinese Academy of Science. His research interests are in discrete conformal geometry, digital geometry processing, and 3D shape analysis.

Wencheng Wang is a professor of the State Key Laboratory of Computer Science, Institute of Software, Chinese Academy of Sciences, where he leads a research group on Computer Graphics and Image Processing. He received his PhD degree in software from Institute of Software, Chinese Academy of Sciences in 1998. His research interests include computational geometry, computer graphics, visualization, and image editing. He is a member of the IEEE and the ACM.